Article

Eisosomes Are Dynamic Plasma Membrane Domains Showing Pil1-Lsp1 Heteroligomer Binding Equilibrium

Agustina Olivera-Couto,[1] Valentina Salzman,[1] Milagros Mailhos,[1] Michelle A. Digman,[2,3] Enrico Gratton,[2,*] and Pablo S. Aguilar[1,*]

[1]Laboratorio de Biología Celular de Membranas, Institut Pasteur de Montevideo, Montevideo, Uruguay; [2]Laboratory for Fluorescence Dynamics, Department of Biomedical Engineering, University of California-Irvine, Irvine, California; and [3]Centre for Bioactive Discovery in Health and Ageing, School of Science and Technology, University of New England, Armidale, Australia

ABSTRACT Eisosomes are plasma membrane domains concentrating lipids, transporters, and signaling molecules. In the budding yeast *Saccharomyces cerevisiae*, these domains are structured by scaffolds composed mainly by two cytoplasmic proteins Pil1 and Lsp1. Eisosomes are immobile domains, have relatively uniform size, and encompass thousands of units of the core proteins Pil1 and Lsp1. In this work we used fluorescence fluctuation analytical methods to determine the dynamics of eisosome core proteins at different subcellular locations. Using a combination of scanning techniques with autocorrelation analysis, we show that Pil1 and Lsp1 cytoplasmic pools freely diffuse whereas an eisosome-associated fraction of these proteins exhibits slow dynamics that fit with a binding-unbinding equilibrium. Number and brightness analysis shows that the eisosome-associated fraction is oligomeric, while cytoplasmic pools have lower aggregation states. Fluorescence lifetime imaging results indicate that Pil1 and Lsp1 directly interact in the cytoplasm and within the eisosomes. These results support a model where Pil1-Lsp1 heterodimers are the minimal eisosomes building blocks. Moreover, individual-eisosome fluorescence fluctuation analysis shows that eisosomes in the same cell are not equal domains: while roughly half of them are mostly static, the other half is actively exchanging core protein subunits.

INTRODUCTION

Compartmentalization of the plasma membrane allows both prokaryote and eukaryote cells to efficiently coordinate essential functions such as cell division and trafficking of materials and information (1,2). Above the micron scale, plasma membrane heterogeneity is evident in eukaryotic-polarized cells where apical and basolateral domains, formed by the polarized trafficking machinery and maintained by tight junctions, ascertain epithelial functional identity (3). Below the micron scale, plasma membrane nanodomains exhibit high diversity of temporal and spatial scales extending from tens to hundreds of nanometers and from milliseconds to minutes and even permanent residency within a cell lifespan (4,5). Our understanding of nanoscale plasma membrane domains composition has been deeply enriched by live microscopy studies using fluorescently labeled proteins and lipids. These studies have unequivocally shown the existence of plasma membrane nanodomains, and their mechanisms of formation, maintenance, and disassembly are under intense debate and study (2,6). Proposed mechanisms focus on confinement within fences formed by membrane proteins anchored to the cytoskeleton, preferential chemical associations among proteins and lipids, and clustering of protein and lipids by membrane-associated scaffolding proteins (2,7).

The plasma membrane of the yeast *Saccharomyces cerevisiae*, contains at least a dozen different nanodomains that exhibit different morphologies and dynamic behaviors (8). Among them, there are topographically distinctive domains, which are shaped as 200–400-nm long and 50-nm-deep invaginated furrows (9,10). Depending on the cell size, there are between 20 and 50 furrows per cell, showing an even distribution and a rather constant density of 0.33 ± 0.06 domains/μm^2 cell surface. These plasma membrane furrows concentrate at least 23 different proteins including nutrient transporters such as Can1 and Tat2 (11,12), membrane-associated signaling proteins such as Pkh1 and Pkh2 kinases (13,14), and the target of rapamycin complex 2 (TORC2) effectors Slm1 and Slm2 (15,16). Two highly abundant membrane-associated proteins, Pil1 and Lsp1, constitute the structural core of these domains (9,17). For each one of these invaginated furrows, it is estimated that 2000–5000 units of both Pil1 and Lsp1 are assembled on the cytoplasmic side of the plasma membrane (17). Pil1 and Lsp1 assemblies have been named “eisosomes” (17) whereas the plasma membrane domains concentrating Can1 and other nutrient

Submitted September 26, 2014, and accepted for publication February 12, 2015.

*Correspondence: pablo.aguilar@pasteur.edu.uy or egratton22@gmail.com

Valentina Salzman’s current address is Instituto de Investigaciones Biológicas, San Martin, Buenos Aires, Argentina.

Editor: Paul Wiseman.

0006-3495/15/04/1633/12 $2.00

http://dx.doi.org/10.1016/j.bpj.2015.02.011

transporters have been named "membrane compartment occupied by Can1" (MCC) (12). Eisosomes and MCCs both constitute the same subcellular structure: the plasma membrane furrowlike invagination. For simplicity, we will use the term "eisosomes" to describe the plasma membrane invaginated furrows and the proteins that partition within. Eisosomes are immobile domains that are formed de novo in the buds of dividing cells (18). The cytoplasmic pools of the core proteins Pil1 and Lsp1 join the plasma membrane of growing buds in a coordinated fashion with other eisosome components. *PIL1* expression oscillates in synchronicity with the cell cycle, matching high expression levels with eisosome formation and buds' plasma membrane growth (18). Pil1 is a major player in eisosomes assembly and maintenance. Deletion of *PIL1* leads to disappearance of furrow membrane invaginations and dramatic relocation of all other known eisosome components: integral membrane proteins spread along the plasma membrane and membrane-associated proteins, including Lsp1, fall into the cytoplasm. In the absence of Pil1, very few and large clusters, referred to as "eisosome remnants", persist at the plasma membrane concentrating a fraction of the original eisosomal proteins (17).

Remarkably, this phenotype is not mimicked by the absence of Lsp1, which is 74% identical in amino-acid sequence to Pil1. Lsp1 and Pil1 are bar/amphyphysin/rvs (BAR) domain-containing proteins able to form a membrane-bound scaffold imposing membrane curvature in vitro and in vivo (19–21). Besides all these extensive studies, the molecular mechanism of eisosome formation and maintenance are still poorly understood. Other eisosome components such as the tetraspanning membrane protein Nce102 and the membrane-associated protein Seg1 are required for efficient incorporation of Pil1 into eisosomes, but their molecular structures and mechanisms of action are still unknown (22,23). Crystallographic studies show that Lsp1, like canonical BAR domain proteins, forms a homodimer in vitro (20). However, whether the cytoplasmic pools of Pil1 and Lsp1 form homo- and/or heterodimers, or even higher-order preassembled units in vivo, remains uncertain. In vitro, Pil1 and Lsp1 are able to directly bind to lipids, but it is unknown whether their cytoplasmic pools are either already bound to intracellular membranes or behave as free diffusing entities. To further contribute to our understanding of eisosome assembly and maintenance mechanisms, we have focused on Pil1 and Lsp1, addressing quantitative aspects of these proteins' dynamics in live cells.

In this work, by using fluorescence fluctuation analytical methods we have determined the dynamic behavior of cytoplasmic Pil1 and Lsp1 in vivo. We have also found that roughly half of the eisosome population contains a dynamic pool of Pil1 and Lsp1. Number and brightness (N&B) and fluorescence correlation spectroscopy (FCS) analysis show that these dynamic pools are oligomeric with slow dynamics that fit with a binding-unbinding equilibrium. Finally, using fluorescence lifetime imaging on live cells, we demonstrated that Pil1 and Lsp1 form heterodimers in the cytoplasm and within the eisosomes.

MATERIALS AND METHODS

The *S. cerevisiae* strains, reagents, media, and growth conditions, Western blotting, microscope setups, mathematics, and data processing are detailed in the Supporting Material.

RESULTS

Eisosome core proteins Pil1 and Lsp1 exhibit diffusive behavior within the cytoplasm

In mitotically active yeast cells, eisosomes are formed de novo in the growing buds by progressive deposition of Seg1, Pil1, Lsp1, and the rest of eisosomal components (18,19,23). Before the bud reaches its final size, well before cytokinesis, deposition of Pil1 (and, presumably, the other major eisosome structural components) has already reached a plateau (18,19). After cytokinesis, when the detached bud turns itself into a novel mother cell, eisosome biogenesis is again initiated toward the new growing bud. Thus, in contrast to growing buds, mother cells contain a population of already assembled eisosomes where the average Pil1-GFP intensity per eisosome remains invariant during a complete cell cycle. It has been previously proposed that, in mother cells, the already assembled eisosomes cores are static; that is, they do not actively exchange core subunits because Pil1-GFP fluorescence recovers very slowly after bleaching (17). However, similar fluorescence-recovery-after-photobleaching experiments performed at physiological temperature (30°C) suggest that, over a time period equivalent to one-half of a cell cycle (45 min), the mother cell's eisosomes exchange ~30% of their Pil1-GFP content (19). To gain a better understanding of the molecular dynamics of already assembled eisosomes, we decided to first characterize their core components in different compartments of mother cells.

For this, we used FCS analysis of temporal fluorescence intensity fluctuations to obtain both high-resolution data on molecular dynamics within a single illumination volume (point-scanning FCS) and positional information of different molecular dynamics (orbit-scanning FCS). Yeast strains bearing single-copy versions of C-terminally tagged Pil1 and Lsp1 driven by their native promoters and located in the natural genomic loci were scanned using a two-photon excitation fluorescence microscope equipped with a photon-counting detector. Point and circular scans were performed on different compartments of mother cells. The trajectory of the circular scans was chosen encompassing the cytoplasm, the plasma membrane, and eisosomes (Fig. 1 *A*).

Control point FCS and orbit-scanning FCS experiments on yeast cells with no fluorescent protein showed minimal autofluorescence and no correlations were detected. On the other hand, control-point FCS experiments with cytoplasmic monomeric Venus (mVenus) expressing cells

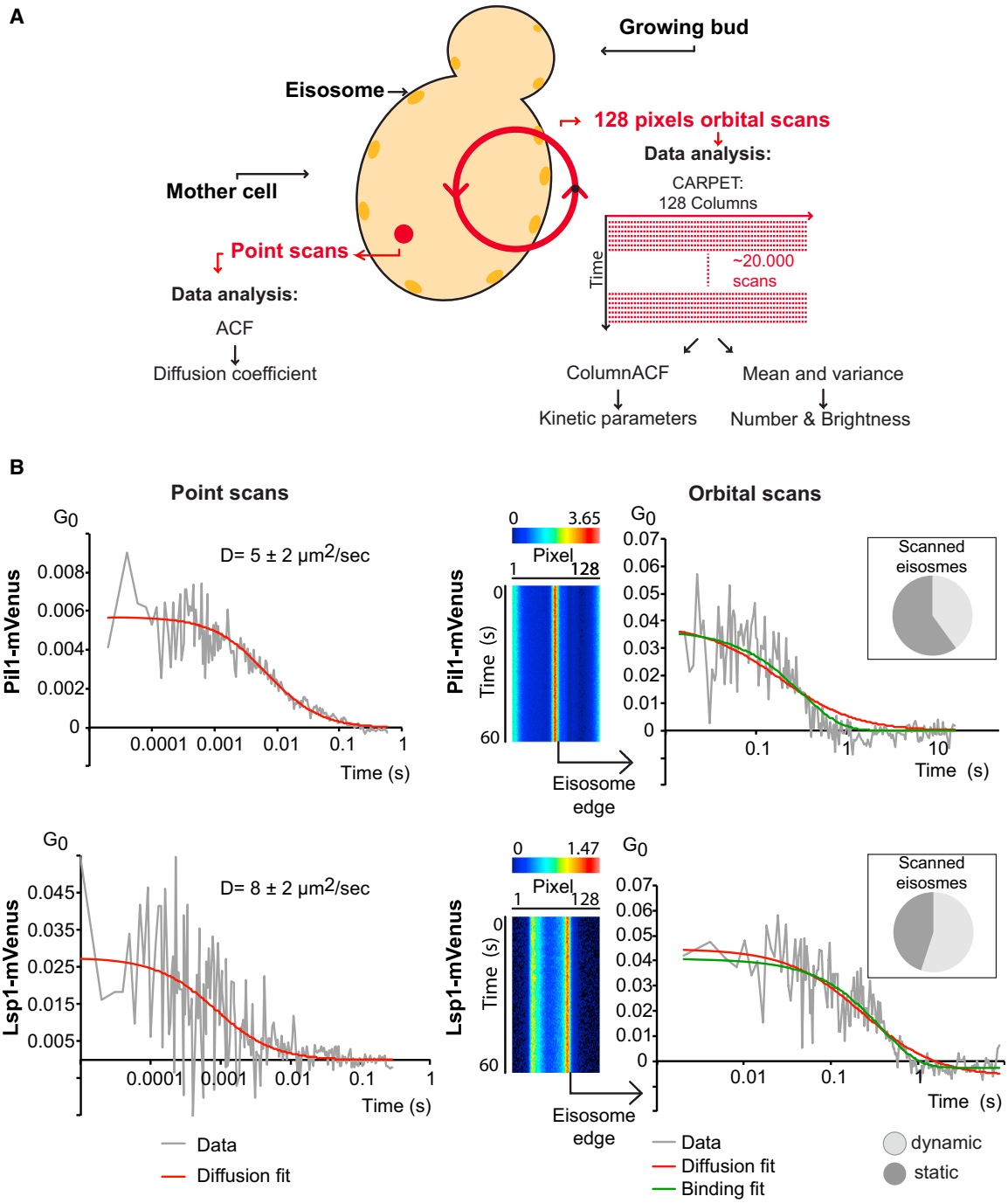

FIGURE 1 ACF analysis of Pil1 and Lsp1 at different subcellular locations. (*A*) Graphic representation of point- and circular-scans-based ACF analysis. Each yeast cell is focused at the equatorial plane and scanned by an immobile beam positioned at the cytoplasm (*point*) or by a circular orbit that passes through an eisosome. (*B*) (*Left panels*) Pil1 and Lsp1 exhibit cytoplasmic free diffusion dynamics. Representative ACF plots and free diffusion fittings of data coming from indicated yeast strains that were subjected to point scans at the cytoplasm. (*Right panels*) Circular scans reveal Pil1 and Lsp1 dynamic populations at the eisosome's edges. Representative fluorescence intensity carpets of Pil1-mVenus and Lsp1-mVenus cells are shown. ACF was calculated for each column/pixel of the carpet. When detected, autocorrelation data was plotted and fitting to free diffusion (*red*) and binding-unbinding equilibrium (*green*) models were tested. (*Insets*) Distribution of dynamic and nondynamic Pil1 and Lsp1 pools over a total of 25 and 20 individually scanned eisosomes, respectively. Parameter values (D_{app}, G_0, K, and A) and fitting statistics of analyzed cells are given in Table S1. To see this figure in color, go online.

evidenced autocorrelation yielding an apparent diffusion coefficient (D_{app}) of 11.2 ± 0.5 $\mu m^2/s$ (Fig. S1), which is consistent with the dynamic behavior of this protein in bacterial cells (24) and of similar fluorescent proteins located in the budding yeast's cytoplasm (25). Data obtained from cytoplasmic point scans of Pil1-mVenus cells were individually fit to a free diffusion model. After fitting analysis, we could determine that cytoplasmic Pil1-mVenus dynamic behavior is compatible with free diffusion exhibiting a D_{app} of 5 ± 2 $\mu m^2/s$ (Fig. 1 *B*, *top-left panel*). Equivalent imaging, processing, and analysis for Lsp1-mVenus cells indicated that, like Pil1-mVenus, the dynamic behavior of Lsp1-mVenus obeys free diffusive kinetics with a D_{app} of 8 ± 2 $\mu m^2/s$ (Fig. 1 *B*, *bottom-left panel*).

A subset of eisosomes exhibits binding-unbinding Pil1 and Lsp1 dynamics

Overall, these results show that cytoplasmic Pil1 and Lsp1 pools behave as relatively free diffusing molecules with D_{app} that are compatible with low aggregation states (monomeric to oligomeric). Point-FCS provides dynamic information at a single spatial location and turned out to be inadequate to obtain meaningful data when sampling at eisosome cores or eisosome edges was attempted. To address the dynamic behavior of Pil1 and Lsp1 we employed orbital scans, which enabled us to simultaneously evaluate different cellular locations (Fig. 1 *A*). Orbital scans have sampling interval times much longer than those used for point-FCS sampling. Although this sampling frequency is too slow to detect free diffusing monomeric molecules like mVenus, it allowed us to detect slower moving particles, which is something we can expect from plasma membrane proteins and/or large complexes within the cytoplasm. To simplify the analysis visualization, the intensity data captured by the scanning orbit is displayed in two-dimensional carpets where the *x* dimension corresponds to each orbit pixel and the *y* dimension corresponds to time (Fig. 1 *B*, *right panels*). Autocorrelation analysis for each point in the orbit (the columns in the carpet) was performed for >20 Pil1-mVenus and >25 Lsp1-mVenus cells registered over three independent experiments. This analysis enabled us to identify a common pattern: autocorrelation was detected in pixels located at the edges of eisosomes and not within them (Fig. 1, *right panel*). Fitting of the autocorrelation function (ACF) was done using a free diffusion null hypothesis model, but results indicated that this model was not fitting the data well. The deficient fittings to a free diffusion model of the ACFs of moving particles located at the eisosomes edges were characterized by a narrowing of the ACFs with respect to the model (see examples for Pil1 and Lsp1 in Fig. 1 *B*). In contrast, all diffusion models, regardless of whether they represent normal, hindered, or anomalous diffusion, will produce a broader ACF. Instead, we have observed a narrowing of the ACF, which is typical of binding equilibrium. Consistently with this hypothesis, an ACF exponential formula characteristic of binding-unbinding equilibrium to an immobile fraction (the eisosome core) provided a better fit in the totality of pixels analyzed, giving mean first-order kinetic constants of 2.9 ± 0.6 s^{-1} for Pil1-mVenus and 3.1 ± 0.9 s^{-1} for Lsp1-mVenus (Table S1).

These results suggest that, within mother cells, both Pil1 and Lsp1 partition in at least three dynamically different populations: 1) an immobile fraction at the eisosome's core, 2) a cytoplasmic free-diffusing fraction with D_{app} compatible with monomeric or low aggregation states, and 3) an eisosome-associated fraction that is dominated by a binding-unbinding equilibrium behavior and localizes at the eisosomes edges. Remarkably, the eisosome-associated dynamic fraction detected at some eisosomes was absent in other eisosomes of cells that were similarly grown and scanned. Orbital-scan measurements and ACF analysis showed that the eisosome-associated Pil1 and Lsp1 dynamic populations were present in 40 and 55% of individually scanned eisosomes, respectively (see Fig. 1 *B*, *insets*, *right panels*). Moreover, for both proteins, these mobile fractions were always detected at the eisosome edges and not at the eisosomes cores. Thus, our results indicate that a subset of mother cell eisosomes is static whereas there is another fraction of eisosomes with boundaries containing dynamic pools of Pil1 and Lsp1.

Number and brightness analysis reveals the aggregation states of the different eisosome core proteins' subcellular pools

Diffusion coefficient values obtained by ACF analysis suggest that cytoplasmic Pil1 and Lsp1 exist as either monomeric or low aggregation states. Moreover, whether the eisosome-associated Pil1 and Lsp1 dynamic pools are either monomeric or preassembled is also uncertain. To address these points, we obtained a cellular map of Pil1 and Lsp1 aggregation states performing N&B analysis over the same temporal intensity fluctuations data analyzed by ACF. N&B is based on moment-analysis that utilizes the average intensity and the variance in the intensity distribution at each pixel to calculate the number (N) of diffusing particles within the illumination volume and their apparent brightness (B) (26). In the simplest case, the molecular brightness ε (where $\varepsilon = B-1$) of an n-mer oligomer is n times the monomer brightness. Thus, providing a pixel-by-pixel map of number and brightness in an image, N&B analysis enables us to determine the oligomerization state/s of proteins in living cells with high spatial resolution (see the Supporting Material for a more detailed description).

Intensity fluctuations data of mVenus-bearing cells were used as the reference of the brightness of the monomeric

fluorophore. Because we used a yeast strain that expresses mVenus from a multicopy plasmid and because the number of copies per genome of this type of expression vectors varies from cell to cell (27), the resulting population of mVenus cells has a wide distribution of mVenus intensities. This cell-to-cell variation in mVenus expression levels enabled us to determine that our brightness calculations were robust over a wide range of fluorescence intensities. Within each experimental set, mVenus brightness histograms were fitted to Gaussian distributions and used to calculate the average monomeric brightness value (Fig. 2 *A*). Pil1-mVenus brightness histograms exhibited a predominant population similar to mVenus and a minor population corresponding to higher brightness values (Fig. 2 *A*). Visual inspection of intensity and brightness values in the expanded orbits carpets, where the *x* dimension corresponds to each orbit pixel and the *y* dimension corresponds to independent measurements, suggested that the cytoplasm is mainly occupied by Pil1-mVenus with the brightness values similar to mVenus whereas higher brightness populations are found at eisosome's edges (Fig. 2 *B*). Similar brightness populations were detected for Lsp1-mVenus (data not shown). On the other hand, the eisosome core immobile fraction displays monomeric brightness values, which were more likely to have originated from fluctuations of the cytosolic pool.

To quantitatively assert the subcellular distribution of the different oligomeric populations, we segmented the orbit scans in three subcellular compartments (cytoplasm, eisosome core, and eisosome plus edges) using the intensity profile of the carpet (Fig. 3 *A*). Then, we classified brightness values in three categories: monomers, oligomers, and multimers, taking mVenus brightness values as a reference (see Fig. 3 *B* and the Supporting Material). The statistical analysis represented as overlapped box and dot plots confirms what is observed in Fig. 2 *B*: in wild-type cells, only 8% of Pil1-mVenus corresponds to oligomers, and multimers are few. Moreover, this analysis reinforces the hypothesis that eisosome edges are populated by a dynamic oligomeric fraction of Pil1, as has already been shown in Fig. 2 *B*. Considering all these results, we interpret the presence of Pil1 oligomers as a dynamic subpopulation that binds and dissociates from eisosomes with a kinetic constant of $2.9 \pm 0.6\ s^{-1}$ (Figs. 1, 2, and 3 and Table S1). We note that fluctuations at both edges of the same eisosome are uncorrelated, ruling out that eisosome movements, as a whole, are responsible for the fluctuations at the eisosomes' edges.

Number and brightness plots provide the opportunity to determine the averaged distance between oligomers and the eisosome core. For this, we selected the number and brightness profiles of all the eisosomes with detected oligomers and fitted N&B profiles to Gaussian distributions (Fig. S2). Mapping of the centers of mass of the resulting Gaussian fits indicated that the mean distance between oligomers and eisosomes is 275 ± 60 nm, a value that resides within the dimensions of eisosomes (200–400-nm long and 50-nm deep). We asked whether this oligomeric population of Pil1 is sensitive to protein concentration. To address this point, we analyzed cells in which a high-copy vector containing *PIL1-mVENUS* was the sole source of Pil1 (see Materials and Methods for more details). Overexpression of Pil1 produces a normal number of eisosomes per cell, but with higher content of Pil1 per eisosome (18). N&B analysis of *PIL1*-overexpressing cells showed that, indeed, an increase in Pil1 protein concentration correlates with the appearance of higher amounts of oligomers and even higher-order assemblies (Figs. S3 and 3 *B*). Quantitative analysis of the cytoplasm fluorescence average intensity and brightness of overexpressed Pil1-mVenus showed that the artificial increment of cytoplasm protein concentration leads to the generation of bigger oligomeric and even multimeric aggregates of Pil1-mVenus within the cytoplasm (Fig. S3 *C*).

Fluorescence lifetime quenching analysis demonstrates that Pil1 and Lsp1 directly interact in the cytoplasm and at eisosomes

Our results indicate that Pil1 and Lsp1 coexist in the cytoplasm of mother cells sharing similar D_{app} (Fig. 1). Immunoprecipitation of whole-cell extracts followed by mass spectrometry analysis shows that both proteins physically interact in a close to equimolar relationship (17). In vitro, both proteins Pil1 and Lsp1 are able to form homodimers and high-order macromolecular assemblies (19–21). Despite all this evidence, it is still unknown whether the eisosome core proteins interact directly in live cells.

To address this point, we first asked whether *LSP1* deletion changes Pil1's cytoplasmic aggregation state. Previously, it has been shown that in the absence of Lsp1, there is a slight decrease in the number of eisosomes per cell (0.7-fold) and moderate increases in Pil1-GFP cytoplasmic and eisosome contents (1.8-fold and 1.7-fold, respectively), indicating that Pil1 by itself is still able to form wild-type-like eisosomes (17,18,22). Regardless of the mild phenotype of eisosomes' organization showed by *lsp1*Δ cells, N&B analysis of Pil1-mVenus revealed a more specific phenotype (Fig. S4). When compared with wild-type cells, N&B maps and box plots of *lsp1*Δ cells showed an overall increase in Pil1-mVenus brightness values. This increase is evident at eisosome edges and it is also detected within the cytoplasm (Fig. S4). These results, indicating that the lack of Lsp1 leads to an increase in the cellular content of Pil1 with higher brightness values, suggest that Pil1 homo-aggregation replaces Pil1-Lsp1 heterodimers that normally exist in wild-type cells.

To challenge this hypothesis, we performed Förster resonance energy transfer (FRET) experiments between Pil1 and

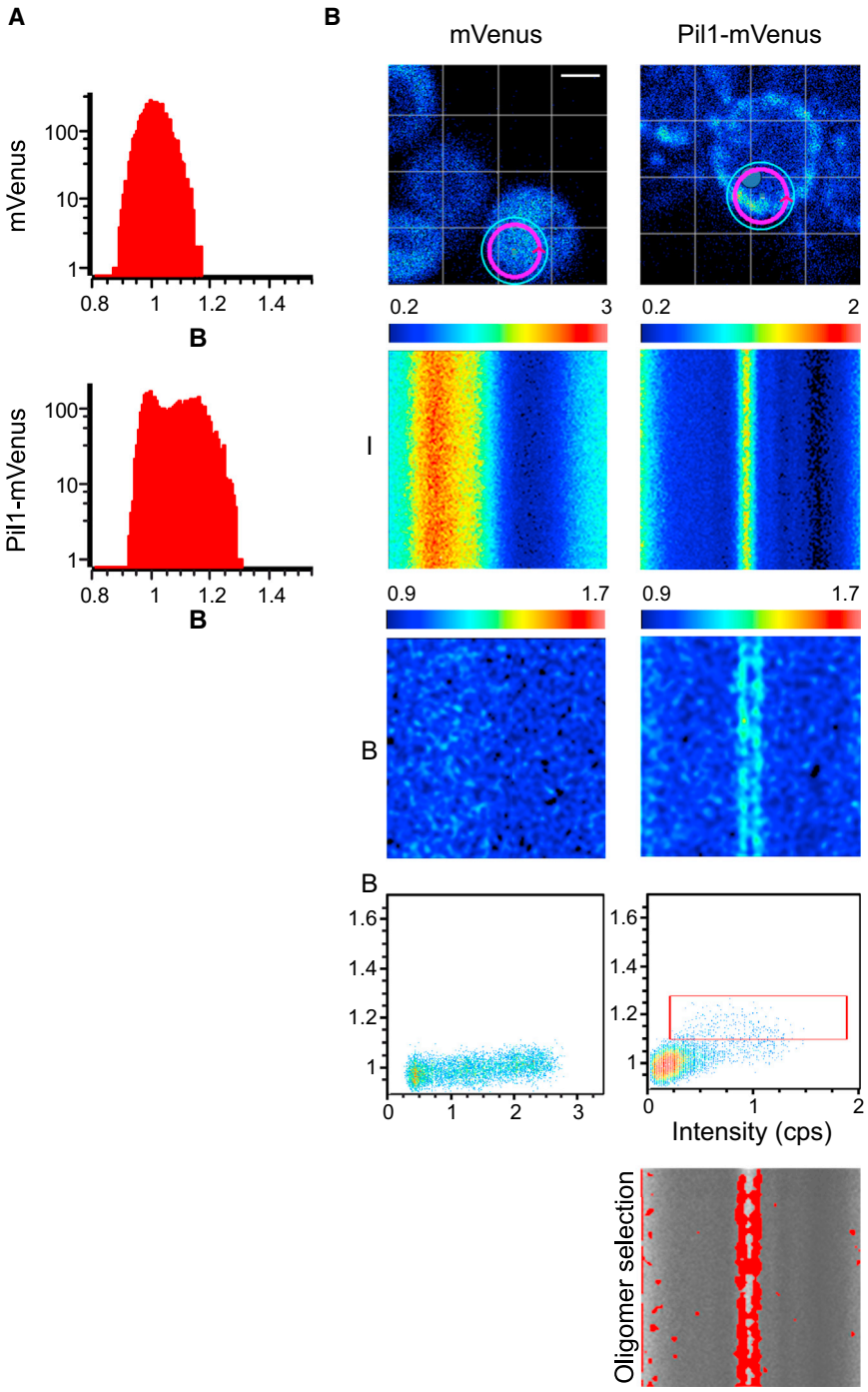

FIGURE 2 Pil1 presents different oligomer states depending on its subcellular localization. Yeast strains carrying either mVenus or Pil1-mVenus were subjected to circular scans and N&B analysis. (*A*) Apparent brightness histograms of one representative cell. (*B*) First-row panels show representative images of cells scanned with circular orbits (*magenta circular line*; *arrowhead*, scan starting point). The second- and third-row panels display corresponding carpets with intensity (*I*) and brightness (*B*) values. Each carpet is composed of 128 columns representing each pixel of the orbit and 128 rows, each one corresponding to an independent set of measurements (see the Supporting Material for more detail). Intensity carpet for Pil1-mVenus cell presents two eisosomes with cores at columns 1–4 and 59–63. Fourth-row panels show brightness- versus intensity-plots; (*red box*) selected pixels with brightness values higher than monomeric mVenus (for a more detailed explanation of oligomer selection, see the Supporting Material). These pixels are false-colored (*red*) in the grayscale B-carpets (*bottom panel*). Scale bar: 2 μm. To see this figure in color, go online.

Lsp1 using both possible combinations of donor- (mVenus) and acceptor- (mCerulean) tagged proteins in live cells. To detect FRET and to measure its efficiency, we used the donor's lifetime quenching as the readable output. Fluorescence-lifetime-imaging microscopy (FLIM) measurements were performed by image acquisition in the frequency domain and represented using the phasor approach (28). In this approach, the donor's fluorescence lifetime in each pixel of the FLIM raster scan is represented in a two-dimensional polar plot (the phasor plot). In the case of FRET, quenching of the donor's fluorescence lifetime is evidenced by displacement of the lifetime pixel population within the phasor plot (Fig. 4 *A*). Thus, comparison of donor-only with donor-acceptor phasor plots allows the detection of shifts in lifetime pixel populations due to FRET. Moreover, quantitative evaluation of FRET efficiencies (Table 1) can be performed without fitting to exponential models (28,29). Phasor plots representing the totality of cellular

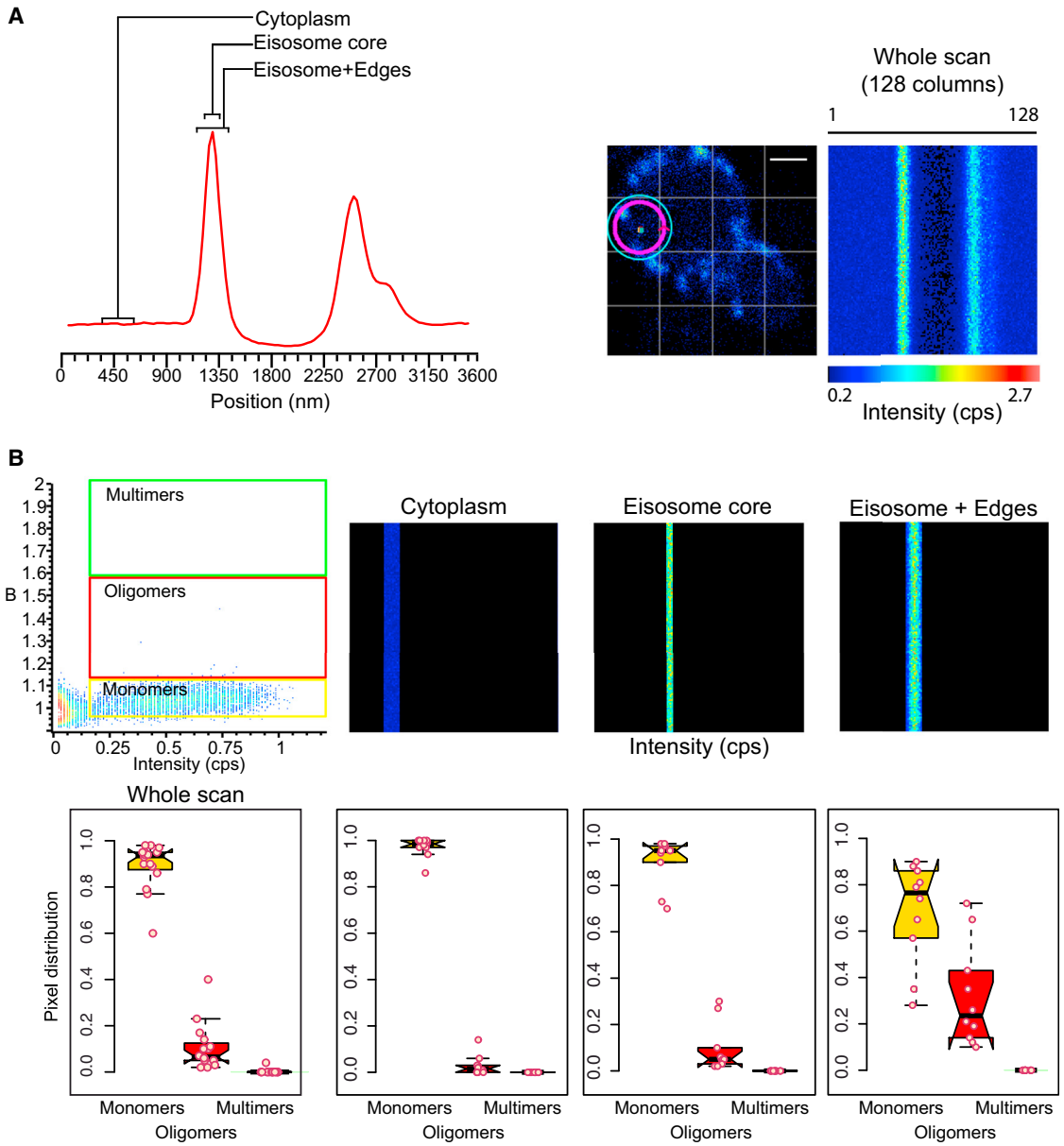

FIGURE 3 Pil1 aggregation states subcellular quantitation. (*A*) Subcellular compartments definition criteria. (*Red*) Intensity profile of a 128-pixel circular scan of a Pil1-mVenus yeast cell. Eisosome core consists of a 212-nm-wide area encompassing the intensity center of mass. Eisosome edges are defined as the eisosome core's contiguous 159-nm-wide areas and the cytoplasmic compartment is defined as the central 530-nm-wide area of cytoplasmic signal (for a more detailed explanation, see the Supporting Material). Scale bar: 2 μm. (*B*) Monomeric, oligomeric, and multimeric ranges of brightness values were defined in relation to mVenus brightness-value distributions (for a more detailed explanation, see the Supporting Material). Intensity value (I-) carpets for each subcellular compartment as defined in (*A*) are shown. Boxplots show the statistical analysis of the pixel distribution belonging to each species in the whole scan and within each subcellular compartment as defined in (*A*). Data from three independent experiments with at least six cells per experiment were analyzed. To see this figure in color, go online.

pixels showed a clear decay in the donor lifetime, indicating that Pil1 and Lsp1 directly interact in vivo (Fig. 4 *A*, *two left panels*). To identify the subcellular source/s of the FRET signal we filtered the pixels into cytoplasm, eisosomes, and eisosome edge compartments (Fig. 4 *B*). In all cases, filtered pixels were displaced toward lower lifetime values, indicating that Pil1-Lsp1 direct interaction occurs in all subcellular compartments (Fig. 4 *C*, *two left panels*).

This result was independent of the protein donor carrier protein and, moreover, we observed higher FRET efficiency when the mCerulean carrier was Lsp1 (Fig. 4 *C* and Table 1). Considering unquenched mCerulean lifetimes in donor-only strains and autofluorescence, we calculated the FRET efficiencies for the donor-acceptor strains (see the Supporting Material for details). Table 1 summarizes the different FRET efficiencies for the complete set of

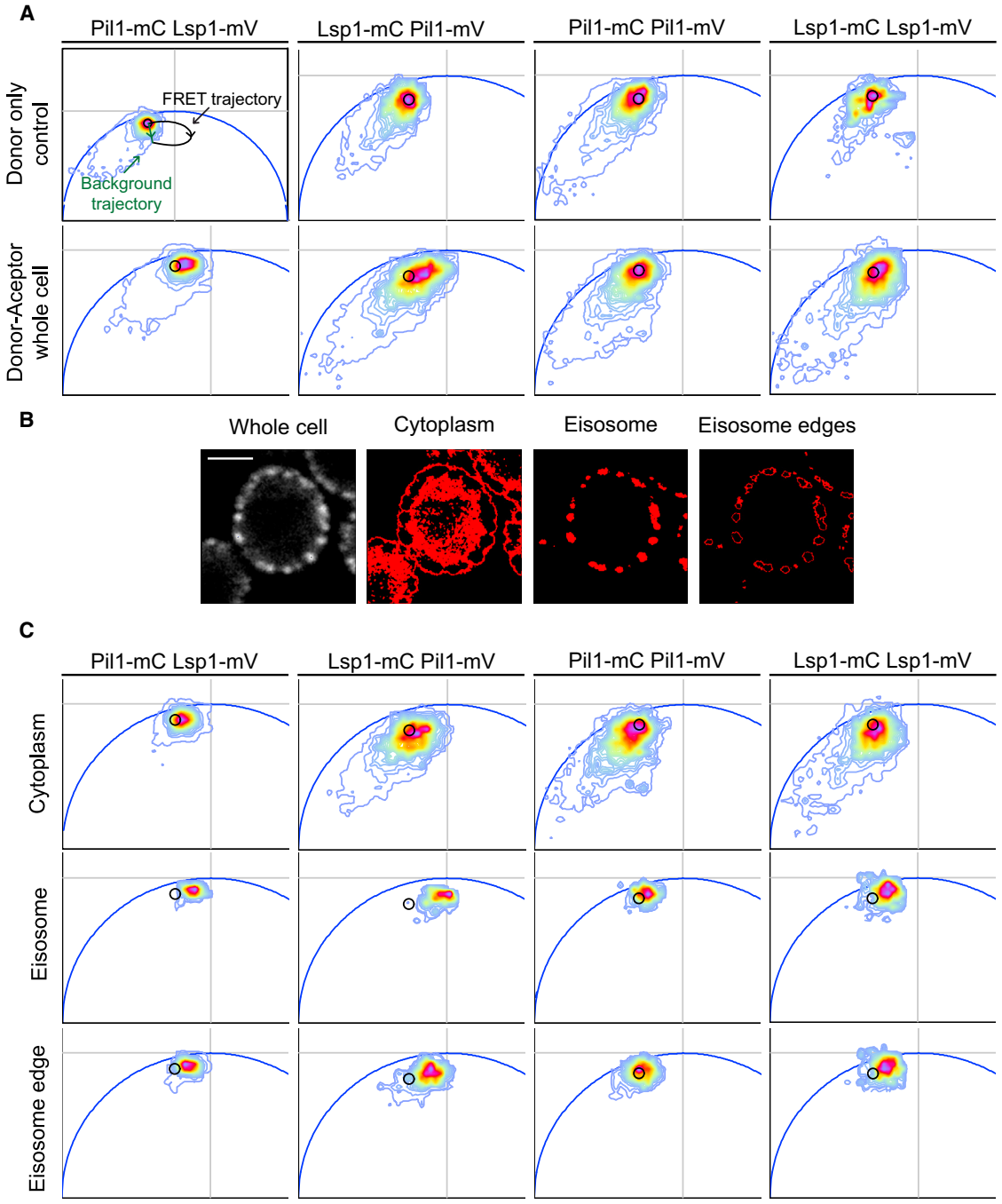

FIGURE 4 FLIM-FRET analysis of Pil1 and Lsp1 direct interactions in vivo. All possible combinations of mCerulean- and mVenus-tagged Pil1 and Lsp1 strains were imaged with a two-photon microscope equipped with a FLIMbox (ISS, Champaign, IL) and results were analyzed using the phasor plot approach. (*A*) Phasor distribution of lifetimes measured in cells expressing the fluorescent donor-only controls (Pil1-mCerulean or Lsp1-mCerulean) or donor-acceptor pairs. A theoretical FRET trajectory (*black curved arrow*) and a background trajectory (*green arrow*) are shown within the Pil1-mCerulean donor-only phasor plot (*upper-left*). The trajectory originates at the black circle (which represents 0% FRET efficiency), whereas the trajectory's end corresponds to 100% FRET efficiency. The black circle is concentric to the donor-only pixel distribution center-of-mass, and encompasses 80% of the pixels. This circle is repeated in phasor plots above as a visual reference of the donor-only center-of-mass position. (*B*) Example of fluorescence-intensity-based subcellular compartments segmentation. Scale bar, 2 μm. (*C*) Phasor plots of pixels' lifetimes corresponding to the subcellular compartments as defined in (*B*). All phasor plots presented with pixel distribution lifetimes were built from the integration of six or more cells in each plot. From violet until red color, one standard deviation of the pixel dispersion is comprehended, and two standard deviations are contained until yellow. Phasor plots are shown zoomed-in for better visualization. To see this figure in color, go online.

TABLE 1 FRET efficiencies

Strain	Whole cell	Eisosome	Eisosome edge	Cytoplasm
Pil1-mC Lsp1mV	5	10	10	5
Lsp1mC-Pil1mV	12	20	17	12
Lsp1-mC Lsp1-mV	20	30	20	0
Pil1-mC Pil1-mV	10	20	15	0
Pil1-mC Pil1-mV *lsp1*Δ	5	28	18	10

Yeast strains expressing the different possible donor-acceptor FRET pairs were imaged for fluorescence lifetime data acquisition (see the Supporting Material for detail). For each strain, pixel distribution lifetimes coming from at least six different cells were integrated within the same phasor plot. FRET trajectories in the phasor plots were calculated and, for each subcellular segmentation, the FRET efficiency of the center of mass of pixel distribution in the phasor plot was calculated using the FRET calculator of SIMFCS (Globals Software, Laboratory for Fluorescence Dynamics, http://www.lfd.uci.edu/globals/). See Figs. 4 and S5 for visual inspection of phasor plots for center-of-mass positions and pixel population dispersions.

analyzed cells, discriminating among the different subcellular regions.

Thus, our point-FCS (Fig. 1), N&B (Figs. 2 and 3), and FLIM-FRET results strongly suggest that the cytoplasm of wild-type cells is populated by Pil1-Lsp1 heterodimers. However, these findings do not rule out the existence of a more complex scenario where Pil1-Pil1 and/or Lsp1-Lsp1 homodimers also contribute to eisosome structure. To address this possibility, we constructed heterozygote diploid strains containing either Pil1-mCerulean/Pil1-mVenus or Lsp1-mCerulean/Lsp1-mVenus pairs (Table S2) and performed live FLIM-FRET experiments. Phasor plots of the whole cellular signal showed decreases in the donor lifetime in Lsp1-Lsp1 pairs (Fig. 4 *A*, *right panel*) and, to a lesser extent, in Pil1-Pil1 pairs as well (Fig. 4 *A*, *third panel*). Phasor plot of the different subcellular compartments showed a donor lifetime reduction in eisosome and eisosome-edge pixels, but not in cytoplasmic pixels (Fig. 4 *C*, *right panels*). Calculated FRET efficiencies for both homo pairs across different cellular compartments confirm the lack of homotypic interaction in the cytoplasm and the presence of Pil1-Pil1 and Lsp1-Lsp1 interactions at eisosomes and eisosome edges (Table 1). We interpret the existence of homotypic interactions to be a result of higher-order assembly of Pil1-Lsp1 heterodimers at eisosomes and eisosomes' edges.

DISCUSSION

Using a complementary set of fluorescence fluctuation analysis methods, we have systematically addressed the dynamic properties of eisosome core proteins Pil1 and Lsp1 in live cells. In a simplistic view, eisosome assembly occurs in daughter cells (growing buds), whereas, in mother cells, already-assembled eisosomes are in a steady state. In this work, we focused on Pil1 and Lsp1 behavior within the cytoplasm and eisosome compartments of mother cells. Further work will be directed toward the understanding of eisosome assembly in daughter cells.

Based on several examples of our experimental evidence, we propose that the Pil1-Lsp1 heterodimer constitutes the eisosome's minimal building block, as follows. First, Pil1-mVenus (molecular mass 65.8 kDa) and Lsp1-mVenus (molecular mass 65.5 kDa) cytoplasmic populations exhibit D_{app} (5 ± 2 $\mu m^2/s$ and 8 ± 2 $\mu m^2/s$, respectively) that, when compared with mVenus (molecular mass 27.5 kDa, $D_{app} = 11 \pm 0.2$ $\mu m^2/s$), are compatible with dimeric or low aggregation states (Fig. 1). Second, live FLIM-FRET results indicate Pil1 and Lsp1 directly interact in the cytoplasm and eisosomes (Fig. 4 and Table 1). Third, similar FLIM-FRET experiments detected Pil1-Pil1 and Lsp1-Lsp1 homotypic interactions only where assembled scaffolds and oligomers are present (Fig. 4 and Table 1). Because the Pil1-Pil1 donor-acceptor pair does exhibit positive FRET signals at cytoplasmic pixels in *lsp1*Δ cells (Fig. S5 and Table 1), we reason that negative FLIM-FRET results for Pil1-Pil1 cytoplasmic homotypic interaction in wild-type cells cannot be attributed to insufficient closeness and/or orientation of the donor and acceptor dipoles. Fourth, N&B analysis of Pil1-mVenus and Lsp1-mVenus in wild-type cells detected cytoplasmic brightness values equivalent to mVenus only (Figs. 2 and 3, and data not shown). Although we cannot rule out the possibility that a fraction of cytosolic Pil1 and/or Lsp1 may exist in a monomeric state, the cytoplasmic dominance of monomeric brightness values for both proteins is better interpreted as arising from Pil1-Lsp1 heterodimers. Based on ACF and N&B analysis, we calculate the concentration of Pil1-Lsp1 cytoplasmic heterodimers to be ~400–800 nM. Thus, our results suggest that the cytoplasm of mother cells contain mainly Pil1-Lsp1 heterodimers in the nanomolar concentration range. Both point and orbital scans were applied to mother cells carrying small- to mid-size buds, and therefore, our estimations integrate cells that transit the G2/M phase. This is relevant in the context of eisosome biogenesis, which is cell-cycle-regulated and occurs in correlation with a burst of Pil1 total protein levels during G2/M phase (18). However, as of this writing, whether Pil1-Lsp1 cytoplasmic heterodimers levels fluctuate during the cell cycle, and growing buds are occupied by similar Pil1-Lsp1 cytoplasmic species and concentrations, is unknown.

Although orbital scans were performed over a wide range of sampling intervals (488–122 Hz), we were unable to detect autocorrelation of fluorescence fluctuations at eisosome cores. However, the presence of Pil1 and Lsp1 mobile fractions immediately located next to eisosome highest-intensity pixel values indicates that already-built eisosomes are not completely static assemblies, but instead exhibit heterogeneous dynamics. ACF analysis suggests that both Pil1 and Lsp1 eisosome-associated mobile fractions follow first-order binding-unbinding kinetics with similar rate constants (Fig. 1). Brightness values indicate the existence of similar

aggregation states for both proteins, and FLIM-FRET results indicate that Pil1 and Lsp1 directly interact at eisosomes borders, where oligomers are located (Fig. 4). Taken altogether, our results support the idea that the independently observed Pil1 and Lsp1 oligomers belong to the same dynamic entity.

Which is the subcellular compartment where Pil1-Lsp1 oligomers partition? As of this writing, whether it is the plasma membrane or the cytoplasm is unknown. Because oligomers are not detected further away from eisosomes, it seems unlikely that they partition within the cytoplasm. Quantification of the most probable distances between the eisosomes' centers of mass and oligomers give values within the range of eisosome dimensions. Because of the comparable dimensions of the point-spread function (PSF) of our scanning system (300-nm axial diameter) and eisosome dimensions, we acknowledge that eisosomes can be encompassed by a single PSF. However, Gaussian fits for N&B distributions locate brightness centers away from eisosome centers of mass within a distance that is comparable with PSF axial diameter (Fig. S2). Therefore, we propose that oligomers are located at or near to eisosome edges. Taken together, the binding-equilibrium-dominated kinetics and the short-range location area suggest that oligomers are plasma-membrane-bound entities. In this view, steady-state eisosomes exchange Pil1-Lsp1 oligomeric subunits composed by Pil1-Lsp1 heterodimers that are still attached to the plasma membrane. Either total-internal-reflection-fluorescence microscopy coupled to ACF analysis or super-resolution live imaging techniques compatible with single-particle tracking should help to clarify this issue.

Remarkably, orbital scans, ACF, and N&B analysis of eisosomes with similar intensity profiles show that not all, but a subset, contains dynamic Pil1-mVenus and Lsp1-mVenus oligomers (Fig. 1 *B*, *right panel insets*). Thus, we can distinguish at least two different populations of mother cells' eisosomes: one where the main structural proteins remain static, and one where what we call an "active population" is being remodeled (and which is evidenced by the presence of mobile oligomers). This can explain why different fluorescence-recovery-after-photobleaching experiment analyses alternatively reported zero recovery and small but significant recovery of Pil1-GFP fluorescence after photobleaching (17,19). Because our measurements provide a local snapshot of the complete cell, we do not know whether active eisosomes remain as such, or if they switch to an alternative state with no structural proteins exchange.

An attractive speculation is that these two eisosome populations reflect the dynamic partition within the plasma membrane of different cellular events. Consistent with this idea, work on Slm1 and Slm2 indicates that these signaling proteins, which mediate TORC2-dependent control of lipid homeostasis, colocalize with a subset of eisosomes. Moreover, this discrete localization pattern is dynamic and responds to plasma membrane stress caused by membrane stretch or sphingolipids synthesis inhibition (16). Pil1 and Lsp1 are multiphosphorylated proteins, and their phosphorylation status depends on the activities of the Pkh1/2-Ypk1/2 and Pkc1 kinases' signaling pathways (13,30,31). Pkh2 concentrates in plasma membrane foci that are restricted to a subset of eisosomes (22). *PKH2* (and also *PKH1*) overexpression leads to Pil1 and Lsp1 hyperphosphorylation and to eisosomes disassembly (14). It is proposed that hyperphosphorylation of Pil1 and Lsp1 obliterates the capacity of positively charged residues to interact with the plasma membrane. Pil1 and Lsp1 membrane binding depends in part on positively charged residues that interact with phosphatidylinositol (4,5)-biphosphate (PI(4,5)P2), and are located within their BAR domains (21). PI(4,5)P2 depletion, like Pkh kinases overexpression, leads to eisosome disassembly strongly suggesting that protein-lipid electrostatic interactions are paramount to maintain eisosome core proteins cohesion within the plasma membrane (21). It has been previously demonstrated that eisosomes are needed for PI(4,5)P2 phosphatases Inp51 and Inp52 recruitment to the plasma membrane (32).

It has been recently demonstrated that the PI(4,5)P2 phosphatase Inp51 is recruited within a subset of eisosomes (33). Taking all these observations together, it seems evident that eisosomes are not homogeneous regarding different signaling molecules' recruitment. Thus, it is tempting to speculate that active eisosomes might be sites where either Inp51 and/or Pkh2 concentrate and therefore modify the plasma membrane composition and/or structural proteins leading to eisosome remodeling. Although there is no evidence showing that active eisosomes are the sites where signaling molecules such as Slm1/2 and Pkh2 transiently concentrate, these separate observations still argue in favor of the specialization of eisosomes as sites of specific signaling events.

This study highlights the value of combined fluorescence fluctuation analysis methods in defining the dynamics of eisosomes and their constitutive proteins. Much as single-cell experiments have begun to reveal many novel aspects of cell-to-cell variation, our single-eisosome analysis underlines the capacity of FCS methods to interrogate functional diversity within apparently homogeneous subcellular structures. Further work combining these methodologies and others related, such as super-resolution- and total-internal-reflection-fluorescence-FCS, will be crucial to uncover functional relationships between eisosomes and the different signaling pathways that dynamically locate within.

SUPPORTING MATERIAL

Supporting Materials and Methods, six figures and two tables are available at http://www.biophysj.org/biophysj/supplemental/S0006-3495(15)00171-X.

AUTHOR CONTRIBUTIONS

A.O.-C. performed all the experiments described in the study with help from V.S. (strains construction) and M.M. (strains verification). A.O.-C. processed and analyzed the data with input from E.G., P.S.A., and M.A.D. P.S.A. and A.O.-C. conceived the project, guided the experiments, and wrote the article with input from E.G.

ACKNOWLEDGMENTS

We thank Alejandro Colman-Lerner for reagents, Alessandro Rossetta for helpful advice in data processing, and Laura Estrada Leonel Malacrida, and members of the Gratton and Aguilar laboratories for scientific advice and comments on the article.

This work was supported by the Agencia Nacional de Investigación e Innovación de Uruguay (grant No. FCE-3-2011-1-5942 and Travel Fellowship to P.S.A. and A.O.-C.), the Programa de Desarrollo de Ciencias Básicas, the MERCOSUR Structural Convergence Fund (Fondo para la Convergencia Estructural del MERCOSUR, FOCEM, COF 03/11), the National Institutes of Health (grants No. NIH P41-GM103540 and No. NIH P50-GM076516 to E.G. and M.A.D.), the Journal of Cell Science Traveling Fellowship (to A.O.-C.), a Wood/Whelan Fellowship from the International Union of Biochemistry and Molecular Biology (to A.O.-C.), and Master and Doctoral fellowships from Sistema Nacional de Becas (to M.M. and A.O.-C., respectively).

SUPPORTING CITATIONS

References (34–37) appear in the Supporting Material.

REFERENCES

1. Matsumoto, K., J. Kusaka, …, H. Hara. 2006. Lipid domains in bacterial membranes. *Mol. Microbiol.* 61:1110–1117.
2. Simons, K., and J. L. Sampaio. 2011. Membrane organization and lipid rafts. *Cold Spring Harb. Perspect. Biol.* 3:a004697.
3. Tanos, B., and E. Rodriguez-Boulan. 2008. The epithelial polarity program: machineries involved and their hijacking by cancer. *Oncogene.* 27:6939–6957.
4. Kusumi, A., K. G. Suzuki, …, T. K. Fujiwara. 2011. Hierarchical mesoscale domain organization of the plasma membrane. *Trends Biochem. Sci.* 36:604–615.
5. Eggeling, C., C. Ringemann, …, S. W. Hell. 2009. Direct observation of the nanoscale dynamics of membrane lipids in a living cell. *Nature.* 457:1159–1162.
6. Bagatolli, L. A., and O. G. Mouritsen. 2013. Is the fluid mosaic (and the accompanying raft hypothesis) a suitable model to describe fundamental features of biological membranes? What may be missing? *Front. Plant Sci.* 4:457.
7. Olivera-Couto, A., and P. S. Aguilar. 2012. Eisosomes and plasma membrane organization. *Mol. Genet. Genomics.* 287:607–620.
8. Spira, F., N. S. Mueller, …, R. Wedlich-Söldner. 2012. Patchwork organization of the yeast plasma membrane into numerous coexisting domains. *Nat. Cell Biol.* 14:640–648.
9. Strádalová, V., W. Stahlschmidt, …, J. Malinsky. 2009. Furrow-like invaginations of the yeast plasma membrane correspond to membrane compartment of Can1. *J. Cell Sci.* 122:2887–2894.
10. Moor, H., and K. Mühlethaler. 1963. Fine structure in frozen-etched yeast cells. *J. Cell Biol.* 17:609–628.
11. Malínská, K., J. Malínský, …, W. Tanner. 2003. Visualization of protein compartmentation within the plasma membrane of living yeast cells. *Mol. Biol. Cell.* 14:4427–4436.
12. Grossmann, G., M. Opekarová, …, W. Tanner. 2007. Membrane potential governs lateral segregation of plasma membrane proteins and lipids in yeast. *EMBO J.* 26:1–8.
13. Zhang, X., R. L. Lester, and R. C. Dickson. 2004. Pil1p and Lsp1p negatively regulate the 3-phosphoinositide-dependent protein kinase-like kinase Pkh1p and downstream signaling pathways Pkc1p and Ypk1p. *J. Biol. Chem.* 279:22030–22038.
14. Walther, T. C., P. S. Aguilar, …, P. Walter. 2007. Pkh-kinases control eisosome assembly and organization. *EMBO J.* 26:4946–4955.
15. Grossmann, G., J. Malinsky, …, W. Tanner. 2008. Plasma membrane microdomains regulate turnover of transport proteins in yeast. *J. Cell Biol.* 183:1075–1088.
16. Berchtold, D., M. Piccolis, …, R. Loewith. 2012. Plasma membrane stress induces relocalization of Slm proteins and activation of TORC2 to promote sphingolipid synthesis. *Nat. Cell Biol.* 14:542–547.
17. Walther, T. C., J. H. Brickner, …, P. Walter. 2006. Eisosomes mark static sites of endocytosis. *Nature.* 439:998–1003.
18. Moreira, K. E., T. C. Walther, …, P. Walter. 2009. Pil1 controls eisosome biogenesis. *Mol. Biol. Cell.* 20:809–818.
19. Olivera-Couto, A., M. Graña, …, P. S. Aguilar. 2011. The eisosome core is composed of BAR domain proteins. *Mol. Biol. Cell.* 22:2360–2372.
20. Ziółkowska, N. E., L. Karotki, …, T. C. Walther. 2011. Eisosome-driven plasma membrane organization is mediated by BAR domains. *Nat. Struct. Mol. Biol.* 18:854–856.
21. Karotki, L., J. T. Huiskonen, …, T. C. Walther. 2011. Eisosome proteins assemble into a membrane scaffold. *J. Cell Biol.* 195:889–902.
22. Fröhlich, F., K. Moreira, …, T. C. Walther. 2009. A genome-wide screen for genes affecting eisosomes reveals Nce102 function in sphingolipid signaling. *J. Cell Biol.* 185:1227–1242.
23. Moreira, K. E., S. Schuck, …, P. Walter. 2012. Seg1 controls eisosome assembly and shape. *J. Cell Biol.* 198:405–420.
24. Elf, J., G. W. Li, and X. S. Xie. 2007. Probing transcription factor dynamics at the single-molecule level in a living cell. *Science.* 316:1191–1194.
25. Slaughter, B. D., J. W. Schwartz, and R. Li. 2007. Mapping dynamic protein interactions in MAP kinase signaling using live-cell fluorescence fluctuation spectroscopy and imaging. *Proc. Natl. Acad. Sci. USA.* 104:20320–20325.
26. Digman, M. A., R. Dalal, …, E. Gratton. 2008. Mapping the number of molecules and brightness in the laser scanning microscope. *Biophys. J.* 94:2320–2332.
27. Futcher, A. B., and B. S. Cox. 1984. Copy number and the stability of 2-micron circle-based artificial plasmids of *Saccharomyces cerevisiae*. *J. Bacteriol.* 157:283–290.
28. Digman, M. A., V. R. Caiolfa, …, E. Gratton. 2008. The phasor approach to fluorescence lifetime imaging analysis. *Biophys. J.* 94:L14–L16.
29. Hinde, E., M. A. Digman, …, E. Gratton. 2012. Biosensor Förster resonance energy transfer detection by the phasor approach to fluorescence lifetime imaging microscopy. *Microsc. Res. Tech.* 75:271–281.
30. Luo, G., A. Gruhler, …, R. C. Dickson. 2008. The sphingolipid long-chain base-Pkh1/2-Ypk1/2 signaling pathway regulates eisosome assembly and turnover. *J. Biol. Chem.* 283:10433–10444.
31. Mascaraque, V., M. L. Hernáez, …, M. Molina. 2013. Phosphoproteomic analysis of protein kinase C signaling in *Saccharomyces cerevisiae* reveals Slt2 mitogen-activated protein kinase (MAPK)-dependent phosphorylation of eisosome core components. *Mol. Cell. Proteomics.* 12:557–574.
32. Murphy, E. R., J. Boxberger, …, K. Kim. 2011. Pil1, an eisosome organizer, plays an important role in the recruitment of synaptojanins and amphiphysins to facilitate receptor-mediated endocytosis in yeast. *Eur. J. Cell Biol.* 90:825–833.
33. Fröhlich, F., R. Christiano, …, T. C. Walther. 2014. A role for eisosomes in maintenance of plasma membrane phosphoinositide levels. *Mol. Biol. Cell.* 25:2797–2806.

34. Dalal, R. B., M. A. Digman, …, E. Gratton. 2008. Determination of particle number and brightness using a laser scanning confocal microscope operating in the analog mode. *Microsc. Res. Tech.* 71:69–81.

35. Janke, C., M. M. Magiera, …, M. Knop. 2004. A versatile toolbox for PCR-based tagging of yeast genes: new fluorescent proteins, more markers and promoter substitution cassettes. *Yeast.* 21:947–962.

36. Unger, T., Y. Jacobovitch, …, Y. Peleg. 2010. Applications of the restriction free (RF) cloning procedure for molecular manipulations and protein expression. *J. Struct. Biol.* 172:34–44.

37. Digman, M. A., C. M. Brown, …, E. Gratton. 2008. Paxillin dynamics measured during adhesion assembly and disassembly by correlation spectroscopy. *Biophys. J.* 94:2819–2831.